Is the western North Pacific subtropical high a necessary condition for heat waves over the mid-lower reaches of the Yangtze River?

Yixuan Guo[1] · Zuntao Fu[1]

Abstract

Heat waves (HWs) can pose a serious threat to human health and natural ecosystems. Meanwhile, the mid-lower reaches of the Yangtze River are known as one of the most vulnerable regions suffering such disasters. At the mention of their potential drivers, the western North Pacific subtropical high (WNPSH) has been widely accepted as the key atmospheric circulation regulating these high-temperature extremes. Although considerable studies have proved the importance of the WNPSH, not enough work pays attention to the HWs which are not caused by the anomalous WNPSH. This study utilizes the instantaneous co-recurrence ratio α based on the Dynamical System (DS) method to quantify the forcing strength from the WNPSH to HWs, and classify HWs into four types according to their value of α and spatial pattern of the 500 hPa geopotential height, as high-α1, 2 and low-α1, 2. Results show that coverage by the WNPSH is not a necessary condition for the formation of HWs, which may also result from the anomalous South Asian high (SAH) and tropical cyclones (TCs), and the value of α can indicate whether the HWs are coupled with the WNPSH or not. Furthermore, the mechanisms behind these anomalous atmospheric systems are also different. The eastward-extended SAH in high-α HWs is associated with the latent heat of local condensation induced by the abnormal rainfall, while accompanied by an eastward-propagating wave train in low-α1. The intensification of the WNPSH in high-α HWs are attributed to both meridional and zonal wave trains originating from the maritime Continent and Western Europe, respectively, and the anomalous TCs in low-α2 are mainly due to the warmer sea surface temperature over the basin-wide equatorial Pacific, which may heat the bottom atmosphere and provide the convective instability.

Keywords Heat waves · Coupling strength · The western North Pacific subtropical high · The South Asian high · Tropical cyclones

1 Introduction

Heat waves (HWs) are extremely high-temperature events lasting for several days, which have drawn increasing public attention in recent years due to their severe impacts on human health, regional ecosystems and varieties of social developments (Johnson et al. 2005; Robine et al. 2008; Gasparrini and Armstrong 2011; Matthews et al. 2017). These hot extremes have been found going through a rapid growth stage under global warming in terms of their frequency, intensity and temporal duration (Ding et al. 2010; Perkins

et al. 2012; Li et al. 2021a, b), and this upward trend is projected to even accelerate in the future (Imada et al. 2018; Lee and Min 2018; Fischer et al. 2021), calling on proper management of the heat-related risk and comprehensive understandings on the mechanisms behind such disasters.

As for the potential mechanisms behind HWs, the western North Pacific subtropical high (WNPSH) has always been considered as one of the most important atmospheric circulations that dominate the HWs in East Asian monsoon region (Wang et al. 2016; Lee and Lee 2016; Chen et al. 2018). For instance, the abnormal hot summers in 2013 and 2016 over eastern China and in 2018 over Korea are all associated with a significant intensification and shift of the WNPSH (Peng 2014; Ding et al. 2018). The anticyclone induced by the WNPSH favors HWs mainly through the following physical processes: (1) by generating strong descending motion and warming the surface via adiabatic heating; (2) by decreasing the local rainfall and

✉ Zuntao Fu
fuzt@pku.edu.cn

1 Laboratory for Climate and Ocean-Atmosphere Studies, Department of Atmospheric and Oceanic Sciences, School of Physics, Peking University, Beijing, China

cloud cover and increasing the short-wave radiation received at the surface; (3) by giving rise to intense warm advection at the western flank of the anticyclone; (4) by influencing the local land-air interaction and strengthening the upward sensible heat due to soil moisture deficit. Although the WNPSH has been widely used to explain the formation and persistence of HWs, there are still some severe HWs occurring without the anomalous WNPSH, indicating that the connection between HWs and the WNPSH may not be stable, and there are some other systems driving these high-temperature extremes.

Compared with extensive studies on the impacts from the WNPSH on HWs, insufficient work is devoted to the HWs which are not induced by the WNPSH, not to speak of the coupling strength between them. The instantaneous metric α from Dynamical System method has been proved useful in many studies when quantifying the interaction between two variables over a given region (Luca et al. 2020a, b; Guo et al. 2022a). Huang et al. (2022) found α between sea surface temperature and sea air temperature can characterize the ENSO diversity properly, and it can also recognize some well-defined sea surface temperature patterns which are usually overlooked by other ENSO indices. Previous studies usually apply this metric to measure the compounding effect in bivariate extremes (e.g. warm-dry, wet-windy extremes, and day-night hot extremes), in fact this metric can also demonstrate the forcing strength from one variable to the other (in our work, from the WNPSH to HWs) as one direction of the coupling strength, which may be unidirectional, bidirectional or more complex. Note that HWs may also have an impact on the WNPSH, but the coupling strength α does not distinguish the direction, and we omit this direction empirically since the scale of HW is much smaller than that of the WNPSH in both spatial and temporal perspective, and consider the WNPSH and HWs as cause and effect, respectively. In this way, we could estimate whether the HWs result from the WNPSH or not, and answer the question 'is the WNPSH a necessary condition for HWs'.

This paper is structured as follows. Section 2 introduces the datasets and methods. Section 3 demonstrates the different spatiotemporal features of HWs with different coupling strength, and whether the WNPSH is a necessary condition for HWs, if not then what other mechanisms lead to the high temperature. At last, we present the drivers of these anomalous systems and a brief discussion and summary are made in Sect. 4.

2 Data and methods

2.1 Study region and datasets

This study mainly focuses on the Heat waves (HWs) over the pentagonal region known as the mid-lower reaches of the Yangtze River, which is depicted in Fig. S1, east of 111° E, between 26° N and 35° N with two different endpoints 120° E and 122.5° E, similarly defined as previous studies (Luo and Lau 2018; Li et al. 2021a, b; Guo et al. 2022a, b). This region serves as one of the most essential socio-economic centers in China, as well as the most densely populated area (Zhu et al. 2011). Unfortunately, it is also remarkably vulnerable to summertime HWs, which usually induce disproportionally severe damage to local society, eco-environment and agriculture (Robine et al. 2008; Gasparrini and Armstrong 2011; Perkins 2015). Therefore, it is of vital importance to understand the underlying mechanisms of HWs to aid accurate prediction and early warning systems. To describe variations of the western North Pacific subtropical high (WNPSH), we adopt geopotential height at 500 hPa over 15° N–40° N and 110° E–150° E (Fig. S1), which is widely applied in previous studies (Zi et al. 2021; Yang et al. 2022). We also examine the performance of stream function and eddy geopotential height at the same level, which is constructed to remove the increase associated with global warming, and results show no significant difference, since the Dynamical System method is not sensitive to non-stationarities, including internal low-frequency variability or varying external forcing (Messori and Faranda 2020).

The daily maximum 2m temperature (Tmax) and geopotential height at 500 hPa (Z500) involved in the calculation of coupling strength are obtained from ERA5 gridded reanalysis (Hersbach et al. 2020), both cover a span from 1981 to 2020 with a horizontal resolution of $0.25° \times 0.25°$. In composite analysis of large-scale atmospheric and oceanic features, we adopt daily geopotential height, zonal and meridional wind, vertical velocity and air temperature at multiple pressure levels from NCEP/NCAR-R1 (Kalnay et al. 1996), and outgoing longwave radiation (OLR) from NOAA (Lee 2014), all with a 2.5° spatial resolution. The Pacific Decadal Oscillation (PDO) index used in this study is provided by WMO Climate Explorer (http://climexp.knmi.nl/start.cgi), and the series of El Niño decaying summers are provided by NOAA Physical Sciences Laboratory (https://psl.noaa.gov). Daily sea surface temperature (SST) is obtained from OISSTv2, covering the same period and with a 0.25° spatial resolution (Reynolds et al. 2002). We note that the compositing maps from NCEP/NCAR-R1 are generally the same as those from ERA5 (figures not shown here), hence we adopt the low-resolution one to save computing time.

In this study, we mainly focus on the boreal summertime season (June–July–August; JJA) from 1981 to 2020. Anomalous fields are defined as departures from the daily climatology of the study period by removing the mean value on each calendar day. To retrieve convinced results, we also apply 5-day moving average filter and find no qualitative change (figures not shown here).

2.2 Definition of heat waves

Although there is no absolutely universal definition of HWs so far, there are some thresholds that have been widely tested and accepted in substantial studies. Here we follow the definition of HWs by Rousi et al. (2022), which contains three perspectives: intensity, describing the temperature ranges reached; duration, describing the temporal persistence; extent, describing the spatial area covered. In this study, we define a HW as follows:

Temperature threshold Tmax should exceed the 90th percentile of its distribution in the studying period based on a centered 15-day window (Fischer and Schär, 2010).

Temporal duration A heat wave has to persist at least 3 consecutive days, with an interruption for no more than 1 day (Perkins and Alexander 2013).

Spatial coverage We define a heat wave when it covers an area of a fraction 0.6 within a $4° \times 4°$ sliding window (Stéfanon et al. 2012). Different fractions and windows are tested and no qualitative difference is found.

It should be pointed out that these criteria are all applied to each grid point, therefore the selected HWs ought to have spatial configurations, not merely a binary time series.

2.3 Quantification of coupling strength

In this study, we apply Dynamical System (DS) method to quantify the coupling strength α between HWs and WNPSH at each time step, by considering Tmax and Z500 as two dynamical systems. DS method originates from the combination of extreme value theory and Poincare recurrences (Lucarini et al. 2012; Faranda et al. 2020), and it takes the observed variable as a dynamical trajectory $x(t)$ in high-order phase-space, which includes both temporal and spatial information, thus is adept in characterizing the evolution of atmospheric flows, which are often chaotic and quasi-periodic, especially in capturing their non-linear features. The point ζ_x on this trajectory denotes a two-dimensional map at a given time over the studying region (see Fig. 2 in Guo et al. 2022a), and we use a logarithmic function $g(x(t), \zeta_x) = -\log[\text{dist}(x(t), \zeta_x)]$ to measure the distance between ζ_x and a point on the trajectory $x(t)$, with 'dist' as the Euclidean Norm. We consider recurrences as those points close to ζ_x, implying their spatial configurations are highly analogous. Note that this function takes large value when the distance approaches 0. Taking the high 98th quantile of the time series $g(x(t), \zeta_x)$ as threshold s_X, we can extract the exceedances $u(t, \zeta) = g(x(t), \zeta) - s_X$, whose cumulative probability distribution $P[u(\zeta_x)]$ converges to the exponential form of a Generalized Pareto Distribution (GPD) function (Faranda et al. 2017):

$$P[u(\zeta_x)] \simeq \exp\left[-\theta(\zeta_x)\frac{u(\zeta_x)}{\sigma(\zeta_x)}\right], \qquad (1)$$

When involving two variables x(t) and y(t) (e.g. Tmax and Z500 in our study), an instantaneous metric α can be calculated to quantify the co-recurrence ratio between them (Huang et al. 2022):

$$\alpha_{x,y}(\zeta_x, \zeta_y) = \frac{\nu[g(x(t), \zeta_x) > s_x | g(y(t), \zeta_y) > s_y]}{\nu[g(x(t), \zeta_x) > s_x]}, \qquad (2)$$

where $\nu[-]$ representing the number of cases satisfying the condition $[-]$. The metric $0 \le \alpha \le 1$ could quantify the extent to which the points close to the given states on two trajectories occurs synchronously at each time step, in other words, the concurrent local similarity of the two variables in phase-space, thus indicating temporal-spatial covariations between two variables over a given region, and may be interpreted as a proper measurement of coupling strength. Note that this index does not imply the direction of causality, since the order of the variables does not affect the value of α, and the relation it indicates may be unidirectional, bidirectional and even more complex. More detailed information about α and DS method can be found in Faranda et al. (2020), Guo et al. (2022a) and Huang et al. (2022). Related Matlab code is provided by Faranda et al. (2020).

Here we define the HWs with α below the threshold of 20th percentile of α distribution for all summertime HWs as low-α ones, and α exceeding 80th percentile as high-α ones (Fig. S2). The choice of such thresholds is a balance between the two-sided requirements of selected samples that can be regarded as extremes and having plenty of events to meet statistical demands. Reasonable variations are tested and there is no qualitative discrepancy found. Time series of α and HWs are shown in Fig. S3.

3 Results

3.1 Different characteristics of high-α and low-α HWs

The general relationship between summertime Tmax over the mid-lower reaches of the Yangtze River and Z500 over the western North Pacific can be revealed in the scatter plots of the region-averaged anomaly of the two variables (Fig. 1a), from which we can find a weakly positive relation between Tmax and Z500 with the correlation coefficient as 0.23. As expected, the Tmax anomaly of HWs chiefly concentrates upon the right section of Fig. 1a, most of which exceed zero value, and the relatively low Tmax may be attributed to the dipolar pattern of air temperature over the study region (Guo et al. 2022a; Huang et al. 2022).

However, the anomaly of Z500 exhibits a much wider range from −60 to 60 m. This phenomenon is more significant for low-α HWs compared with high-α ones (Fig. 1b), implying that the underlying forcing from the WNPSH to HWs may vary from case to case.

The spatial patterns of high-α and low-α HWs also show different configurations (Fig. 2). While low-α HWs mainly appear in the southwestern part of the study region, the highest frequency of high-α HWs centers upon the eastern coastal region, with the lowest frequency appearing in the northwestern part. The pattern of all HWs exhibits a combined feature from both high-α and low-α HWs, with its center located at the central part of the study region. Furthermore, the magnitude of the frequency for high-α HWs is obviously larger than that for low-α ones, indicating that the spatial coverage of high-α ones is more extensive when

comparing with low-α ones, since the number of the selected HWs is generally equal (110 cases for high-α ones and 119 for low-α ones), and correspondingly high-α HWs tend to cause more serious damage to the local development.

There is a large discrepancy in the seasonality between these two kinds of HWs from 1981 to 2020 (Fig. 3). The frequency of high-α HWs exhibits a single-peaked structure and reaches its top in mid-summer, while two peaks are found in low-α HWs with one in early summer and the other one in the late, and the number of low-α HWs in mid-summer is visibly lower. These seasonal features of high-α and low-α HWs are actually related to zonal and meridional shifts of the WNPSH in boreal summer, which will be further discussed in the later Sect. 4.1.

Since the region-averaged Z500 in HWs exhibits large discrepancies (Fig. 1), and coupling strength α does not
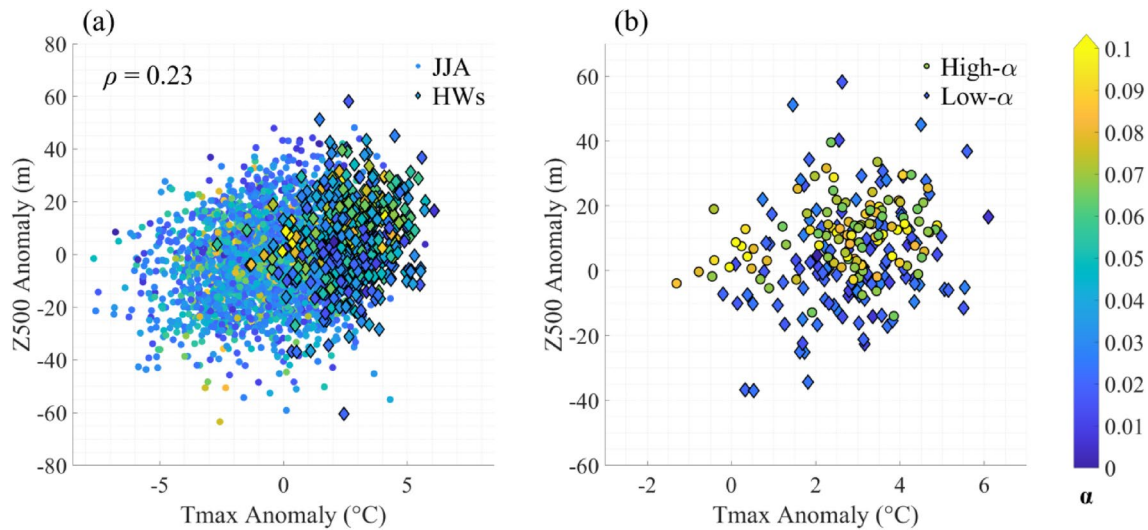
Fig. 1 Scatter plots of the region-averaged anomaly of Tmax versus Z500 for **a** JJA and **b** selected high-α and low-α HWs. The color of the dots denotes the value of coupling strength between Tmax and Z500
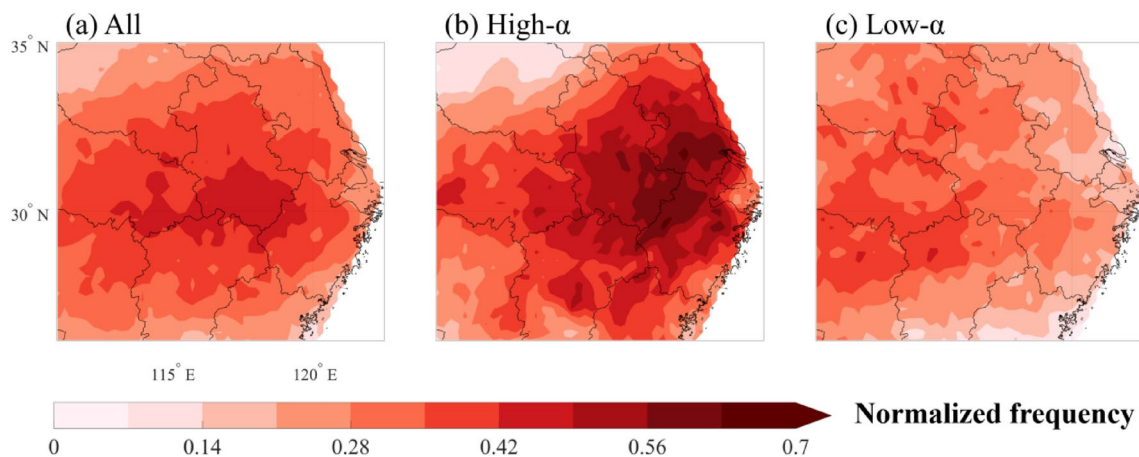
Fig. 2 Frequency of **a** all, **b** high-α and **c** low-α HWs on each grid point normalized by the number of days in the corresponding cluster
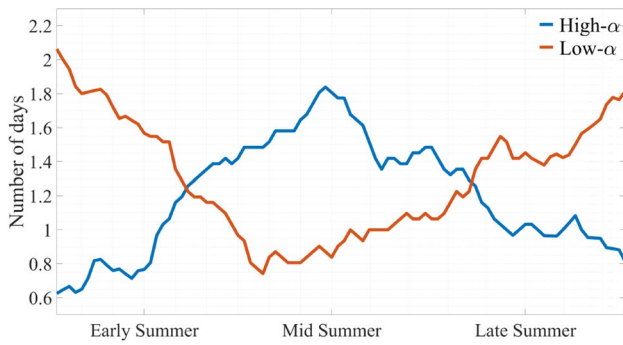
Fig. 3 The number of high-α and low-α HWs occurring on each calendar day in JJA after 31-day running average from 1981 to 2020

differentiate their spatial structures (Guo et al. 2022a), we ought to apply cluster analysis before the later composite analysis to avoid HWs with same α but contrasting patterns offsetting each other. In this study, we utilize *K*-means cluster method to Z500 over the western North Pacific (15° N–40° N, 110° E–150° E) in high-α and low-α HWs, respectively, and use the Calinski–Harabasz criterion to determine the optimal number of groups (Caliński and Harabasz 1974), which is two for both types of HWs. The Calinski–Harabasz value and scatter plots for each type are shown in Figs. S4 and S5. The first cluster of high-α HWs

(hereafter, high-α1) exhibits a meridional dipolar pattern over the mid-lower reaches of the Yangtze River, with its extremely high temperature centered more southward compared with that in high-α2 HWs, in which maximum Tmax is rather located in the northeastern part of the study region (Fig. 4). However, the magnitude of Tmax in low-α1 and low-α2 is slightly smaller relative to high-α HWs, and their extreme centers are biased to the southwest inland, which is consistent with the results shown in Fig. 2. Additionally, we could find positive temperature anomalies over an extensive extent for both high-α and low-α HWs, extending beyond the study region to the western North Pacific and parts of the Tibet Plateau, suggesting that these extreme events are virtually regional disasters instead of local ones, and it is vital to further study such extremes and the possible mechanisms behind them.

3.2 Physical mechanisms behind high-*α* and low-*α* HWs

The WNPSH has been found of great importance in dominating its surrounding weather and climate state, and its intensity, westward extension and meridional shift are also known to have a significant impact on HWs and heavy precipitation over eastern China (Luo and Lau 2017; Zhang et al. 2017; Qiao et al. 2021). The anomalous anticyclone
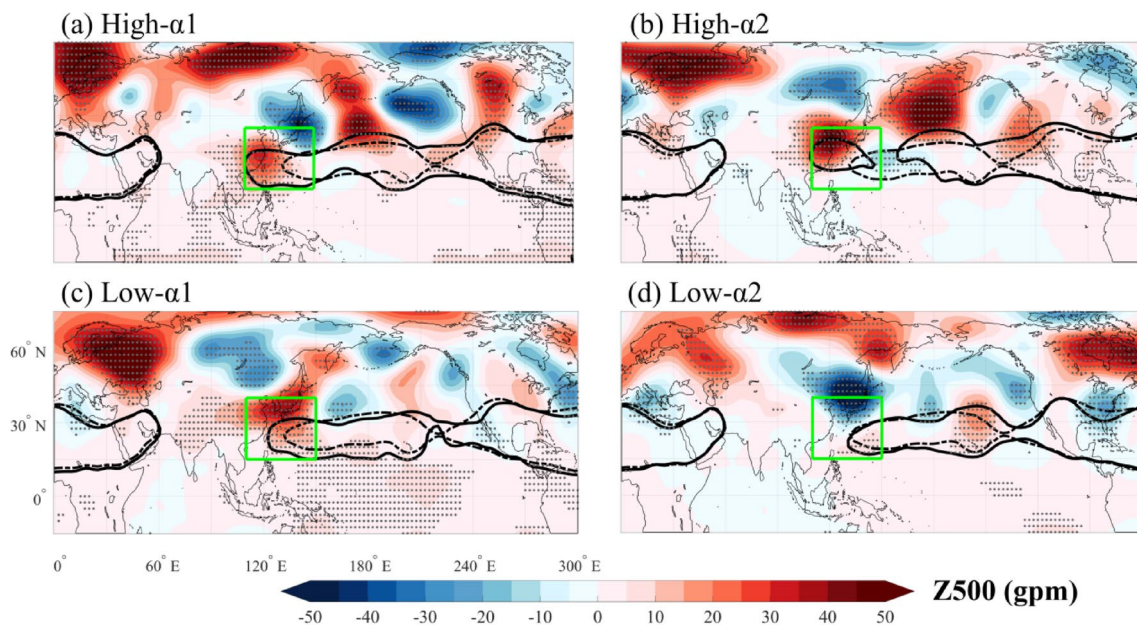
Fig. 4 Composite maps of Tmax anomaly for **a**, **b** high-α and **c**, **d** low-α HWs. Stippling illustrates statistical significance at the 0.05 level by Student's *t*-test. The green pentagon is the location of the mid-lower reaches of the Yangtze River
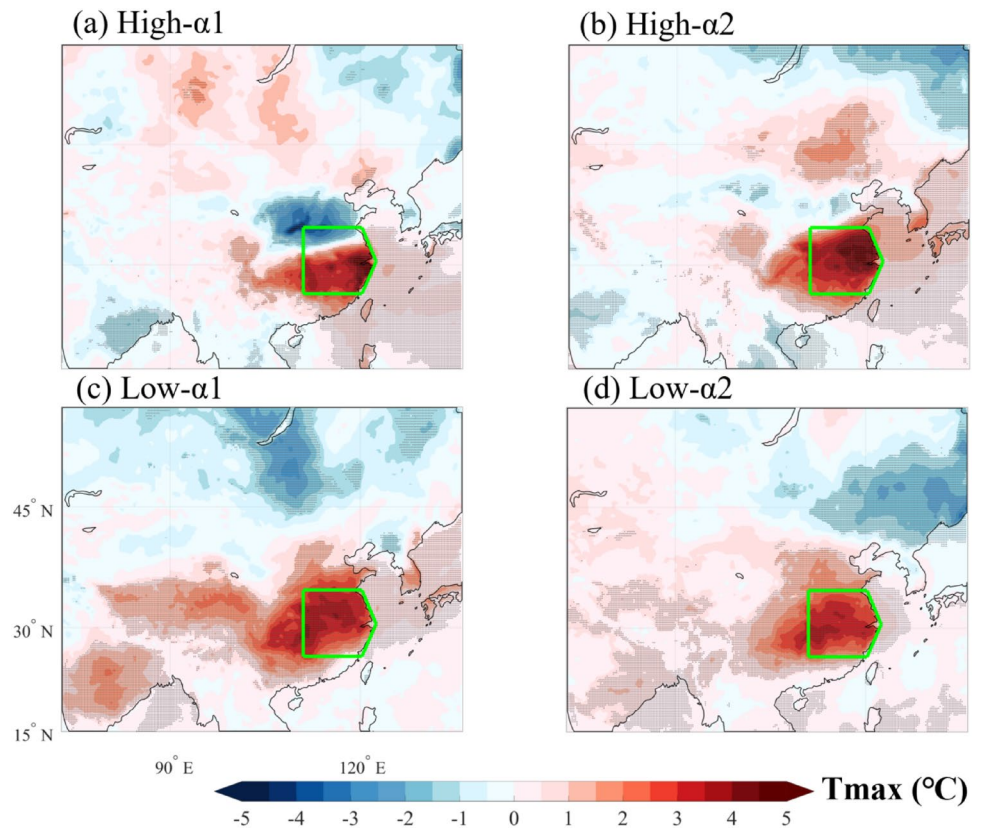
it causes in the middle and low troposphere could directly enhance the descending motion and warm the surface temperature adiabatically, and the associated decrease in rainfall and cloud cover may lead to an increase in net short-wave radiation received and also elevate the surface temperature via diabatic heating. In this study, we choose 5880 gpm as the edge of the WNPSH, and find great enhancement and westward extension of the WNPSH in high-α HWs, with its west endpoints reaching 110° E and almost entirely covering the mid-lower reaches of the Yangtze River (Fig. 5a, b). Significant positive anomaly can be found in both clusters of high-α HWs over the western North Pacific, whereas the center in high-α1 is more southward and in high-α2 more northward, which is highly in accord with the Tmax center shown in Fig. 4, suggesting that the HWs and the WNPSH are strongly coupled in these two clusters. Additionally, there is a low-pressure system cutting off the contiguous WNPSH in high-α2, pushing the west part of the WNPSH moving more northwestward and preventing its eastward withdrawal, thus leading to a prolonged anticyclonic circulation controlling over the Yangtze River Valley, which is favorable for the persistence of HWs. However, the WNPSH in low-α1 still remains at sea with a slight westward extension, and its anomalous positive center appears in Japan and Korea instead of eastern China. Moreover, the Yangtze River Valley in low-α2 is obviously affected by the anomalous trough over the Sea of Japan, which is proved as a northward-moving tropical cyclone (TC) later in this study, without visible influence from the WNPSH. The absence of WNPSH

in low-α HWs demonstrates that these HWs are actually uncoupled with the WNPSH, in other words, overlain by the WNPSH is not a necessary condition for HWs over the mid-lower reaches of the Yangtze River, and the metric α can be utilized to distinguish them from the coupled ones.

Then what mechanism leads to the high temperature in low-α HWs? Previous studies found that the South Asian high (SAH) also plays a key role in regulating the surrounding atmospheric circulations, and its eastward-westward shifts could greatly impact the extreme events over eastern China (Wei et al. 2015; Ding et al. 2018; Shang et al. 2019; Cao et al. 2022). Figure 6 exhibits the anomalous SAH in each cluster, which is represented by 12,520 gpm contour at 200 hPa, and the associated divergence and horizontal winds. The SAH in low-α1 moves a little eastward and covers the southwest part of the mid-lower reaches of the Yangtze River, in line with the location of the highest Tmax in this type of HWs (Fig. 4c). The related convergence caused by the eastward-extended SAH encounters that from the anomalous anticyclone in midlatitudes at around 130° E, and nearly covers the whole area of the study region, thus leading to a strong sinking flow, which may heat the surface both adiabatically and non-adiabatically, and favor the formation of HWs. At the same time, an intensified and very eastward-extended SAH in the upper troposphere can be found in the two clusters of high-α HWs (Fig. 6a, b). Together with the downstream WNPSH stretching westwards at the middle level, these two anomalous high-pressure systems can result in intense subsidence over the study region, then lead to an

Fig. 5 Composite maps of geopotential height anomaly (shading), the 5880 gpm contour (solid line) and its climatology in JJA (dash-dotted line) at 500 hPa. Stippling illustrates statistical significance at the 0.05 level by Student's *t*-test. The green rectangle represents the study region as the western North Pacific
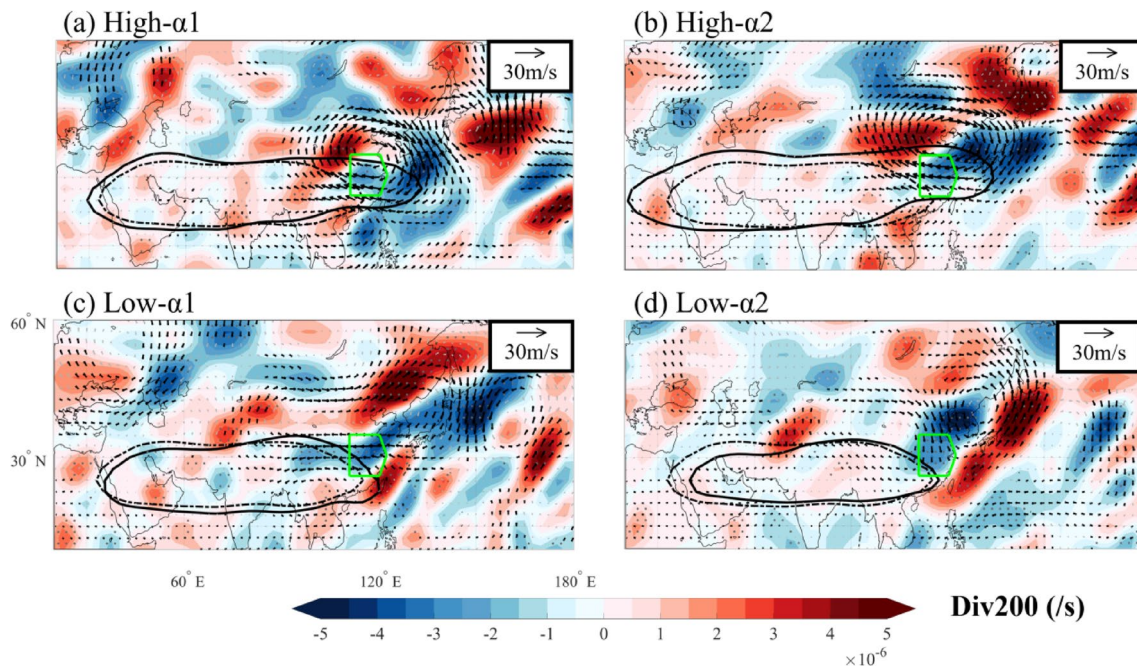
Fig. 6 Composite maps of divergence anomaly (shading), horizontal wind anomaly (vectors), the 12,520 gpm contour (solid line) and its climatology in JJA (dash-dotted line) at 200 hPa. Black vectors denote either zonal or merid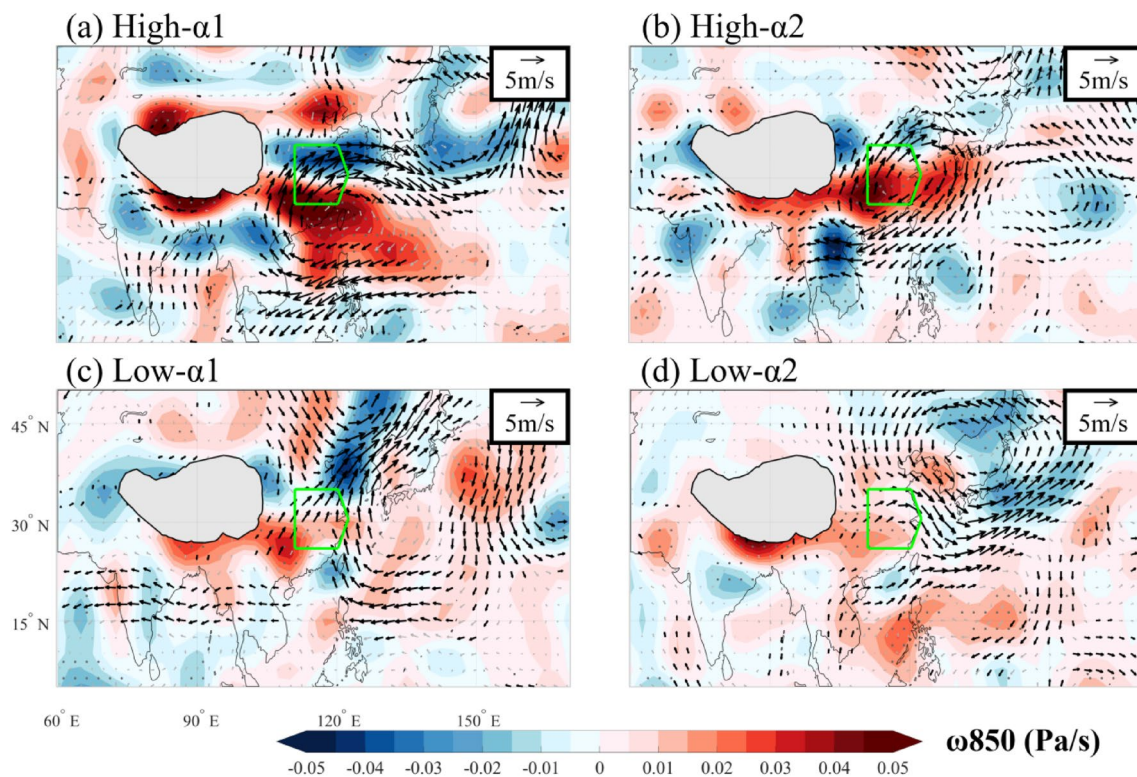ional winds pass the significance test at the 0.05 level by Student's t-test, while gray not. Stippling illustrates statistical significance at the 0.05 level by Student's t-test. The green pentagon represents the study region as the mid-lower reaches of the Yangtze River

extremely high temperature at surface. The relationship of the zonal shift between the WNPSH and SAH is known as the 'face-to-face' displacement or 'back-to-back' departure, which means that a westwards displacement of the WNPSH tends to be accompanied by an eastward shift of the SAH, and vice versa (Tao and Zhu 1964; Zhang et al. 2016). Nonetheless, the SAH in low-α2 does not show much zonal shift, which is weaker than its climatology and shrinks especially at its west boundary. The anomalous convergence in these HWs is mainly caused by the strong cyclonic circulation northeast to the study region, whose center of divergence and horizontal flow are slightly misplaced at the upper level of the troposphere.

In the lower troposphere, we could also find anomalous descending motion in all types of HWs (Fig. 7), where the sinking flow in high-α HWs is attributed to the combined effect from the intensified WNPSH and SAH, while in low-α1 it is caused by the SAH solely, with the anomalous subsidence resulting from the WNPSH lying over the western North Pacific instead of the mid-lower reaches of the Yangtze River. As for low-α2, the extreme subsidence caused by the SAH appears in the southern flank of the Tibetan Plateau, and the positive anomaly in our study region is literally part of the surrounding downdraft around the cyclone centered upon the Sea of Japan, which comes from the tropical region and has been quickly moving to the northwest from ten days ago (Fig. S6). The moving

path from the southeast to the northwest of the negative anomaly has proved that the cyclonic circulation in low-α2 is actually a TC from the tropical western Pacific, instead of an anomalous trough from the upstream mid-latitude. The relatively weaker and larger-scale negative anomaly before day 0 is due to the different tracks of TCs, since we apply K-means cluster analysis to the circulation only on day 0. The surrounding downdraft around a TC may also lead to a decrease in cloud cover and resultant increase in solar radiation, thus providing a favorable condition to generate HWs (Guo et al. 2022b).

To sum up, coverage by the WNPSH is not a necessary condition for HWs over the mid-lower reaches of the Yangtze River, and the coupling strength α computed from Tmax and Z500 can distinguish if the HWs are coupled with the WNPSH. High-α HWs are highly coupled with the intensified WNPSH, with a great impact from the eastward-extended SAH as well, while low-α HWs are uncoupled with the WNPSH, but caused by the SAH solely and the passing-by TCs. These differences can also be revealed in the vertical profile shown in Fig. S7, where the maximum value centers of the anomalous descending motion in high-α HWs are slightly lower at around 700 hPa, affected by the WNPSH which is located in the middle and low troposphere, but appearing at higher than 500 hPa in low-α1, which is exclusively influenced by the SAH. The anomaly in low-α2 is relatively insignificant due to the configuration of the

Fig. 7 Composite maps of vertical velocity anomaly (shading) and horizontal wind anomaly (vectors) at 850 hPa. Black vectors denote either zonal or meridional winds pass the significance test at the 0.05 level by Student's *t*-test, while gray not. Stippling illustrates statistical significance at the 0.05 level by Student's *t*-test. The green pentagon represents the study region as the mid-lower reaches of the Yangtze River, and the gray area represents the Tibetan Plateau, where the 850 hPa is already below the ground

HWs and TCs, whose distance has exceeded the averaging range of the vertical profile.

3.3 Drivers of the anomalous WNPSH, SAH, TCs

In order to further investigate the potential drivers of these anomalous atmospheric systems, we compare sea surface temperature (SST) conditional upon each cluster in Fig. 8. There is a well-organized La Niña-like pattern manifested in high-α2, with a little deformation in high-α1 and low-α1, and an above normal SST anomaly in the Warm Pool. These asymmetric SST configurations could lead to the increase in the SST zonal gradients in the tropical Pacific and the associated enhancement of the rainfall in the maritime Continent, both of which have been found essential for triggering a meridional wave train along the eastern Asia and finally intensifying the WNPSH (Wang et al. 2017; Qiao et al. 2021). These low-latitude signals are more obvious in the outgoing long-wave radiation (OLR) field (Fig. 9), where significant convective activity can be found over the maritime Continent for high-α1, high-α2 and low-α1, and the following positive and negative center over the southern and northern China. The strength and location of these anomalous centers in the three types

of HWs are slightly different, which exactly confirm the strength and location of the WNPSH discussed above. However, the OLR anomaly over the Warm Pool and the coastal region along the western North Pacific is mostly positive in low-α2, and absent of the meridional 'negative–positive–negative' signals (Fig. 9d), but the SST in the basin-wide tropical Pacific is abnormally higher (Fig. 8d), which may heat the bottom layer of the atmosphere and enhance the convective instability locally, thus in favor of the generation of TCs.

In this study, we also apply TN Wave Activity Flux (WAF) first proposed by Takaya and Nakamura (1997) to investigate the Rossby waves in midlatitudes. It is worth noting that there is a strong WAF at 500 hPa originating from the Western Europe and propagating eastward to the downstream along the westerly jet in high-α HWs, though with some vectors insignificant (Fig. 9a, b). The extra energy carried by WAF could also contribute to the intensification of the WNPSH. Whereas, the origination of significant WAF in low-α1 is more southward, located in the Mediterranean region without a clear propagation path, and the energy from high-latitude area mainly propagates to the west North Pacific instead of our study region, and even disappears in low-α2 (Fig. 9c, d). These different features of zonal and
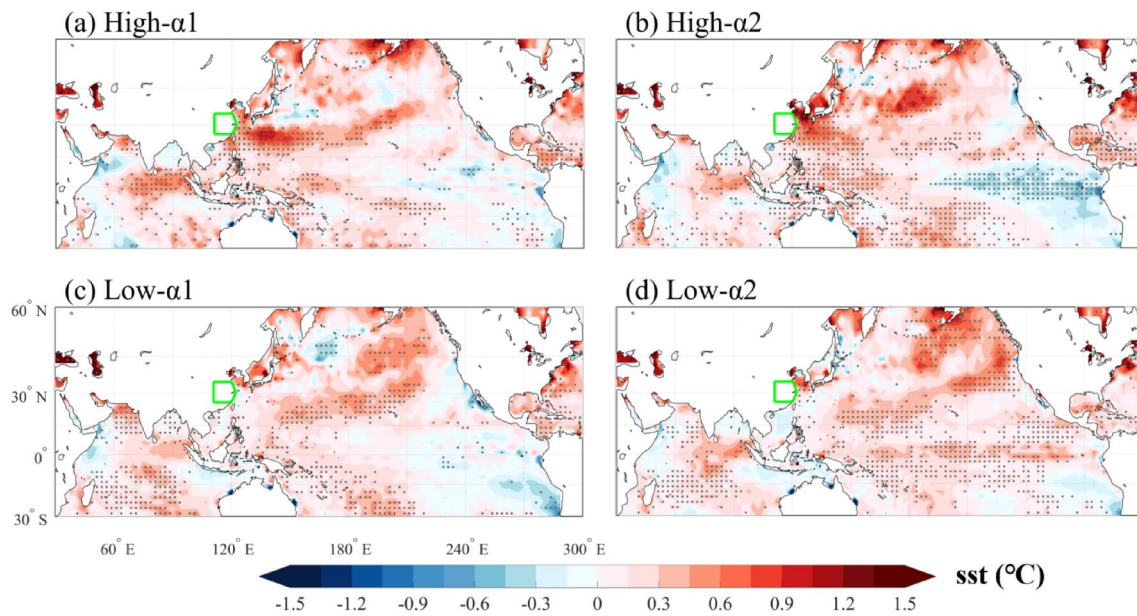
Fig. 8 Composite maps of SST anomaly (shading). Stippling illustrates statistical significance at the 0.05 level by Student's *t*-test. The green pentagon represents the study region as the mid-lower reaches of the Yangtze River
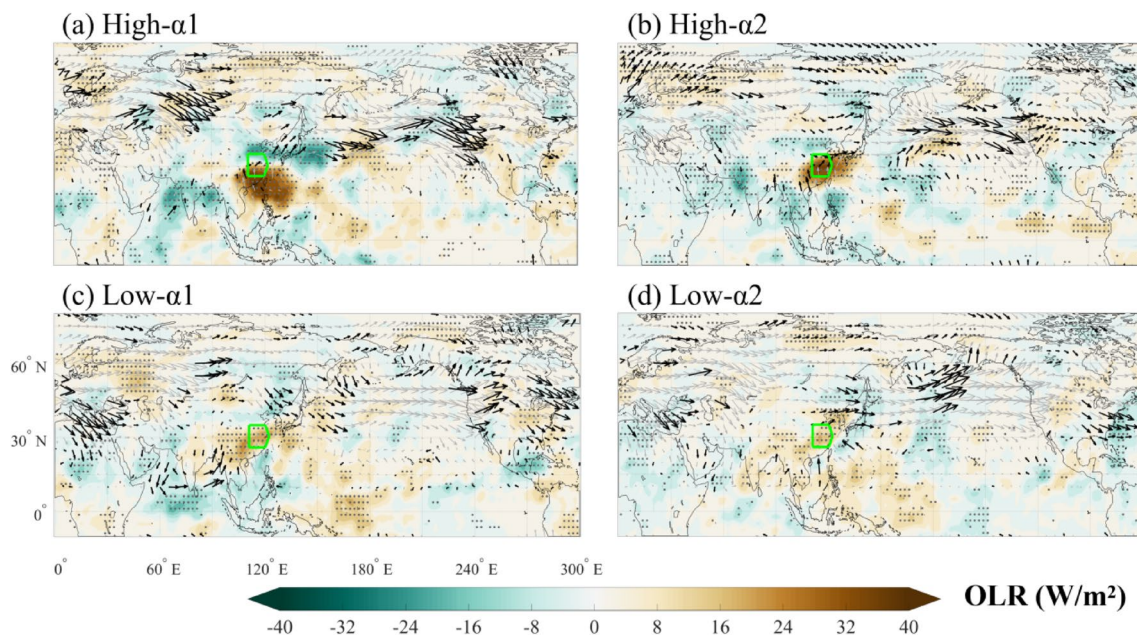
Fig. 9 Composite maps of OLR anomaly (shading) and WAF anomaly at 500 hPa (vectors). Black vectors denote either zonal or meridional WAF pass the significance test at the 0.05 level by Student's *t*-test, while gray not. Stippling illustrates statistical significance at the 0.05 level by Student's *t*-test. The green pentagon represents the study region as the mid-lower reaches of the Yangtze River

meridional wave trains could partly explain the disparity of the WNPSH between high-*α* and low-*α* HWs.

As for the anomalous SAH, previous studies have found that the climatological center of the SAH has a bimodal spatial structure, with one frequent region lying over the Tibetan Plateau and the other one over the Iranian Plateau, both of which have a close interaction with the summertime monsoon (Wei et al. 2014). The excessive rainfall in East Asian and South Asian monsoon region could warm the upper troposphere though condensational heating and excite a local anticyclone at the upper level, thus leading to the eastward and westward extension of the SAH, respectively (Ren et al. 2015; Zhang

et al. 2016; Chen et al. 2022). In high-α HWs, we could find strong convective activity over northern China and most area of the Indian Peninsula (Fig. 9a, b), as well as anomalous ascending motions shown in Fig. 7a, b. The abundant latent heat of condensation induced by the abnormal rainfall may reinforce the geopotential height anomaly locally at the east and west boundary of the climatological SAH, resulting in a great zonal expansion of the SAH as shown in Fig. 6a, b.

However, these abnormal rainfalls are absent in low-α HWs. In fact, the eastward extension of the SAH in low-α1 is associated with the propagation of a wave train across the Eurasian continent (Fig. 10c). The ridge line of the anomalous high-pressure system is located at around 70° E on days -12 and relatively weak at its early stage, then moves gradually from days -12 to -6. The upstream wave trains in the mid-latitudes become legible on days -6, with two positive centers on the south of Lake Baikal and Central Europe, and one significant negative center over the Iranian Plateau. There is also a strong WAF at 200 hPa originating from the central part of North Atlantic, then converging to the center of the eastern anticyclone mentioned above. The inflow of wave energy rapidly strengthens the anomalous high on days -3, and it further gets intensified and reaches its strongest over Northeast Asia on day 0, then splits into two on days $+3$ with one segment still controlling over the mid-lower reaches of the Yangtze River, leading to a favorable environment for prolonged HWs. At its later stage from days -6 to 0, the wave train centers propagate eastward continuously and form an arch shape across the Eurasian continent, which highly resembles the East Atlantic/Western Russia pattern with a slight eastward shift. Compared with the wave train propagating eastward in low-α1, the anomalous high in high-α HWs tends to intensify locally (Fig. 10a, b). The well-defined high-pressure system first appears on days -9 over the Sea of Japan in both clusters of high-α HWs, while in high-α1 it emerges from a weak ridge but in high-α2 it is a merging of two separate anomalous high. Both of them get strengthened and propagate a little westward at the later stage, and entirely cover the study region on day 0. The regional development of the abnormal high without zonal shift confirms the above conclusion that the increased rainfall heats the upper troposphere and induces the enhancement of the SAH via local condensational heating, instead of wave activities from the remote upstream. Nevertheless, there is no visible high-pressure system affecting the study region in low-α2 (Fig. 10d), which is mainly influenced by TCs.

4 Discussions and conclusions

4.1 Discussion

The WNPSH has always been considered as the key system that dominates the HWs over East Asian monsoon region,

but the relationship between the WNPSH and HWs seems not to remain constant. Liu et al. (2019) found that their connection is significantly modulated by the phase changes of the Pacific decadal oscillation (PDO). During the positive phases of the PDO, the strength of the WNPSH and the number of HWs are positively related with a correlation coefficient 0.65, but decreased to 0.12 during the negative phases. Considerable studies have proved that the interannual variability of the WNPSH is influenced by the Indian Ocean (IO) basin-wide SST warming in El Niño decaying summer (Yang et al. 2006; Xie et al. 2009, 2010). During the positive PDO phases, SST in the IO is higher than that during the negative phases, triggering a stronger Kelvin wave propagating eastward and generating a more intense anticyclone in the mid-lower troposphere over the western North Pacific, leading to the enhancement and westward extension of the WNPSH, which favors the formation of HWs over eastern China. In this work, we draw a similar conclusion. During the study period, we find 7 El Niño decaying years with positive PDO phase in total, among which there are 30 high-α HWs but much fewer low-α HWs in 8 days. However, in the 3 El Niño decaying years with negative PDO phase, there is little difference between the number of the two types of HWs, with high-α HWs in 10 days and slightly more low-α HWs in 13 days, suggesting that the value of coupling metric α can distinguish the strength of the connection between the WNPSH and HWs modulated by the phase of PDO. We also examine some other well-known oscillations, such as North Atlantic oscillation, Pacific North American oscillation, Arctic oscillation and Madden–Julian oscillation, but find no noticeable result.

It is well-known that the location of the WNPSH has a significant annual cycle especially in boreal summer, moving northward and westward in early summer, and reaching the northernmost in mid-summer then retreating back at sea in late summer. The different locations of the WNPSH in high-α and low-α HWs in Fig. 5 are nicely consistent with the disparity in the seasonality between the two kinds of HWs shown in Fig. 3, suggesting the robustness of this coupling strength α. As a rule of thumb, we select 5880 gpm as the boundary of the WNPSH similarly defined as previous studies. In fact, if we choose 5860 m as the edge, the study region in low-α1 may also be influenced by the WNPSH. Nonetheless, it does not change the value of the coupling strength α, exactly implying the potential pitfalls of traditional method, by which low-α1 may be classified into the cluster which is caused by the WNPSH, however, our results find that there is only a rather weak causality between these HWs and the WNPSH. It is also worth pointing out that HWs can be caused both dynamically and thermodynamically, and in this study we compute α using Tmax and Z500 over the given region to denote the coupling strength between HWs and the WNPSH from a dynamical perspective, in fact

Fig. 10 Composite maps of geopotential height anomaly (shading), WAF anomaly (vectors), the 12,520 gpm contour (solid line) and its climatology in JJA (dash-dotted line) at 200 hPa in different time lag (− 12, − 9, − 6, − 3, 0 and + 3 days). The green dashed lines represent the ridge line of the high-pressure system affecting the study region. Black vectors denote either zonal or meridional WAF pass the significance test at the 0.05 level by Student's *t*-test, while gray not. Stippling illustrates statistical significance at the 0.05 level by Student's *t*-test. The green pentagon represents the study region as the mid-lower reaches of the Yangtze River
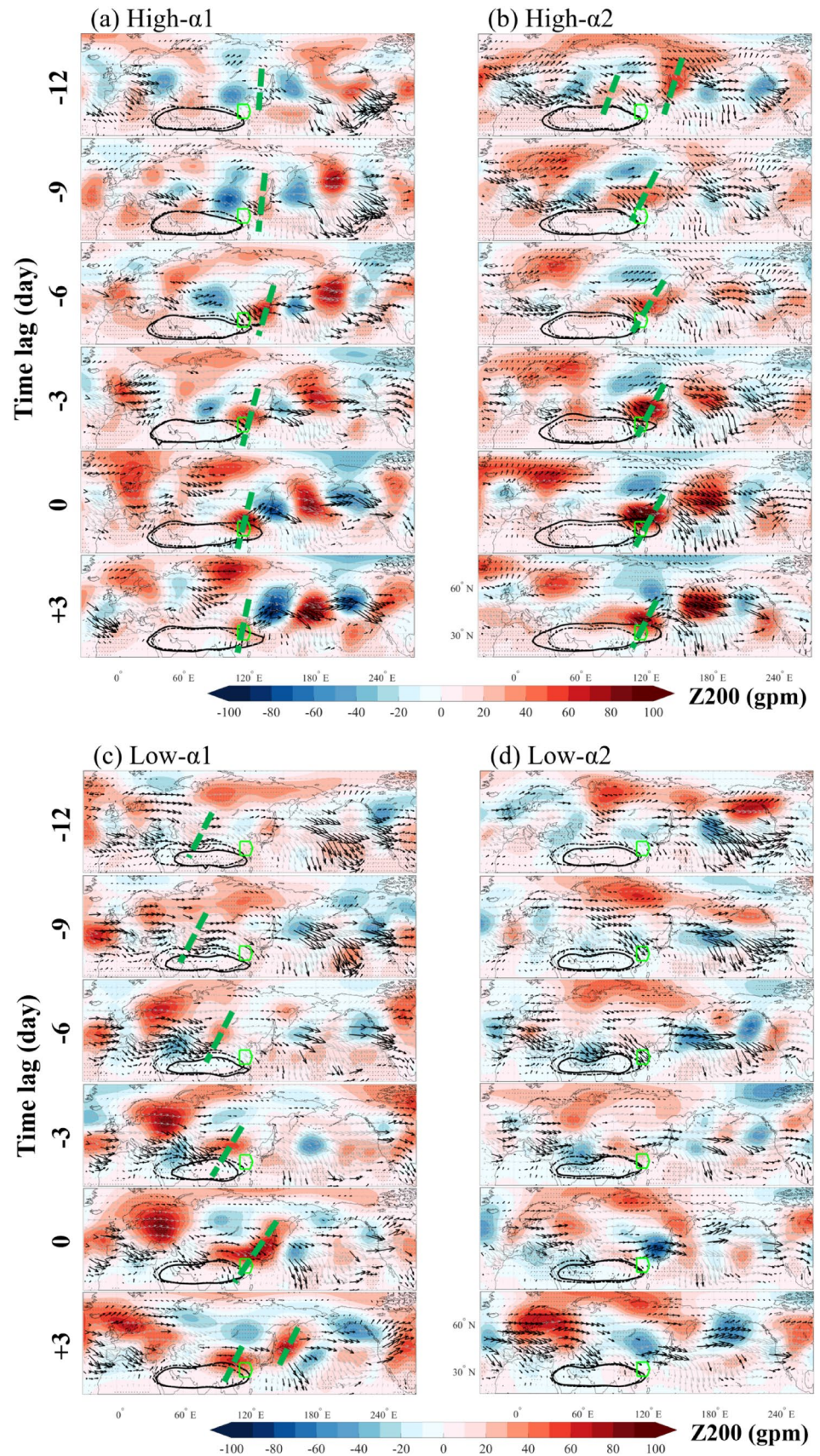
this procedure can be further developed to investigate the relation between HWs and any other systems, for instance, the relation between HWs and the SAH, by replacing Z500 with geopotential height at 200 hPa over the key region of the SAH, or other plausible thermodynamical mechanisms, which provides a novel way to investigate the interaction between two variables with their spatial structures involved.

Using model simulations to investigate HWs is a useful tool and has become a study hotspot recently (Wang et al. 2020; Liao et al. 2021; Hirsch et al. 2021; Xie et al. 2022). Tang et al. (2023) have provided modelling evidence that the anomalous intensified SAH is responsible for the unprecedented 2022 Yangtze River Valley HWs, which is a result of the record-breaking rainfall in Pakistan. To further confirm our results, we also use a historical simulation from EC-Earth3. EC-Earth3 has been found to be the best model simulating HWs over East Asia in CMIP6 (Kim et al. 2020), and it provides geopotential height at 500 hPa simultaneously. We find this historical simulation can reproduce the Tmax and Z500 pattern in the four types of HWs with a slightly smaller magnitude, however, the depiction of the WNPSH in this model is rather inaccurate (figures not shown here). These results indicate that more works are still needed for evaluating the performance of CMIP6 to ascertain the relationship between HWs and large-scale atmospheric circulations found in observations, since previous studies have found that there is differential credibility of climate Modes in CMIP6 (Coburn and Pryor 2021).

4.2 Conclusions

On the basis of DS method, we calculate the dynamical metric α to represent the coupling strength between HWs and the WNPSH by considering Tmax over the mid-lower reaches of the Yangtze River and Z500 over the western North Pacific as two dynamical systems in phase-space, then select the HWs into high-α and low-α ones taking the 80th and 20th percentiles of α distribution of all summertime HWs as the thresholds. We find that high-α HWs are more likely to center upon the eastern coastal region with a larger spatial extent, while low-α ones tend to appear in the southwestern inland and cover a relatively smaller area. As for their temporal features, most of high-α HWs occur in midsummer, whereas there are two peaks for low-α HWs with one in early summer and the other one in late summer. These characteristics in seasonality are related to the location of the summertime WNPSH. We further apply K-means clustering analysis to Z500 over the western North Pacific in order to avoid the potential counteraction caused by different spatial patterns, since the region-averaged Z500 has already shown a large variation. Finally, we obtain four typical clusters of HWs as high-α1, 2 and low-α1, 2.

Through composite analysis, we find that coupled with the WNPSH is literally not a necessary condition for HWs over the mid-lower reaches of the Yangtze River, and the metric α can be utilized to distinguish whether the HWs are caused by the WNPSH or not. For those high-α HWs coupled with the WNPSH, a significant sinking flow can be found over the study region, which is caused by the joint effect of the westward-extended WNPSH and the eastward-extended SAH. However, we could also find descending motion in low-α HWs, but it is attributed to the SAH by itself in low-α1, and being part of the strong downdraft around a TC in low-α2, neither with an obvious impact from the WNPSH. This anomalous subsidence may warm the surface temperature adiabatically, and lead to a decrease in the local cloud cover and a resultant increase in solar radiation, favoring the formation of HWs.

The intensification and westward extension of the WNPSH in high-α HWs mainly results from the excessive wave energy carried by a meridional wave train along eastern Asia, which is triggered by a La Niña-like SST pattern and the associated increase in zonal SST gradients in equatorial Pacific. A zonal WAF over Eurasia continent has also been found convergent to the downstream WNPSH, which helps enhance the WNPSH as well. These meridional and zonal signals are less significant in low-α1, and even disappear in low-α2, where the anomalous TCs are largely due to the warmer SST over the basin-wide tropical Pacific. The underlying drivers of the anomalous SAH in high-α HWs and low-α1 are also different. In high-α HWs, the zonal extension of the SAH arises from the latent heat of condensation induced by the abnormal rainfall over the northern China and the Indian Peninsula, while in low-α1 it is induced by an eastward-propagating wave train along the westerly jet, akin to the East Atlantic/Western Russia pattern with a slight eastward migration.

In this study, we quantify the coupling strength between HWs and the WNPSH, and identify different spatiotemporal features in differently coupled HWs, as well as disparate physical mechanisms. Our results emphasize that the WNPSH is essential but not necessary for HWs, and rather an important role of the SAH and TCs. In the prediction of HWs over the mid-lower reaches of the Yangtze River, we need pay more attention to the interactions between the WNPSH and SAH. This work contributes to the in-depth understandings on the formation of HWs, and helps better predict such disastrous extremes.

Declarations

Conflict of interest The authors declare no competing interests.

References

Caliński T, Harabasz J (1974) A dendrite method for cluster analysis. Commun Stat Theory Methods 3:1–27

Cao D, Xu K, Huang Q, Tam C, Chen S, He Z, Wang W (2022) Exceptionally prolonged extreme heat waves over South China in early summer 2020: the role of warming in the tropical Indian Ocean. Atmos Res 278:106335

Chen R, Wen Z, Lu R (2018) Large-scale circulation anomalies and intraseasonal oscillations associated with long-lived extreme heat events in south China. J Clim 31:213–232

Chen S, Shi W, Wang Z, Xiao Z, Chen W, Wu R, Xing W, Duan W (2022) Impact of interannual variation of the spring Somali Jet intensity on the northwest-southeast movement of the South Asian High in the following summer. Clim Dyn 60:1583–1598

Coburn J, Pryor SC (2021) Differential credibility of climate modes in CMIP6. J Clim 34:8145–8164

Ding T, Qian W, Yan Z (2010) Changes in hot days and heat waves in China during 1961–2007. Int J Climatol 30:1452–1462

Ding T, Gao H, Li W (2018) Extreme high-temperature event in southern China in 2016 and the possible role of cross-equatorial flows. Int J Climatol 38:3579–3594

Faranda D, Messori G, Yiou P (2017) Dynamical proxies of North Atlantic predictability and extremes. Sci Rep 7:278

Faranda D, Messori G, Yiou P (2020) Diagnosing concurrent drivers of weather extremes: application to warm and cold days in North America. Clim Dyn 54:2187–2201

Fischer EM, Schär CM (2010) Consistent geographical patterns of changes in high-impact European heatwaves. Nat Geosci 3:398–403

Fischer EM, Sippel S, Knutti R (2021) Increasing probability of record-shattering climate extremes. Nat Clim Change 11:689–695

Gasparrini A, Armstrong BG (2011) The impact of heat waves on mortality. Epidemiology 22:68–73

Guo Y, Huang Y, Fu ZT (2022a) Regional compound humidity-heat extremes in the mid-lower reaches of the Yangtze River: a dynamical systems perspective. Environ Res Lett 17:064032

Guo Y, Huang Y, Fu ZT (2022b) What causes compound humidity-heat extremes to have different coupling strengths over the mid-lower reaches of the Yangtze River? Clim Dyn. https://doi.org/10.1007/s00382-022-06532-6

Hersbach H, Bell B, Berrisford P, Hirahara S, Horányi A, Muñoz-Sabater J, Nicolas J, Peubey C, Radu R, Schepers D et al (2020) The ERA5 global reanalysis. Q J R Meteorol Soc 146:1999–2049

Hirsch AL, Ridder NN, Perkins SE, Ukkola AM (2021) CMIP6 multi-model evaluation of present-day heatwave attributes. Geophys Res Lett 48:e2021GL095161

Huang Y, Yuan N, Shi M, Lu Z, Fu Z (2022) On the air-sea couplings over tropical Pacific: an instantaneous coupling index using dynamical systems metrics. Geophys Res Lett 49:e2021GL097049

Imada Y, Shiogama H, Takahashi C, Watanabe M, Mori M, Kamae Y, Maeda S (2018) Climate change increased the likelihood of the 2016 heat extremes in Asia. Bull Am Meteorol Soc 99:97–101

Johnson H, Kovats RS, McGregor G, Stedman J, Gibbs M, Walton H, Cook L, Black E (2005) The impact of the 2003 heat wave on mortality and hospital admissions in England. Health Stat Q 25:6–11

Kalnay E, Kanamitsu M, Kistler RE, Collins WD, Deaven DG, Gandin LS, Iredell M, Saha S, White GH, Woollen JS et al (1996) The NCEP/NCAR 40-year reanalysis project. Bull Am Meteorol Soc 77:437–471

Kim M, Yu D, Oh J, Byun Y, Boo K, Chung I, Park J, Park DR, Min S, Sung HM (2020) Performance evaluation of CMIP5 and CMIP6 models on heatwaves in Korea and associated teleconnection patterns. J Geophys Res Atmos 125:e2020JD032583

Lee HT (2014) Climate algorithm theoretical basis document (C-ATBD): outgoing longwave radiation (OLR)—daily. NOAA's Climate Data Record (CDR) Program, CDRP-ATBD-0526 46

Lee W, Lee M (2016) Interannual variability of heat waves in South Korea and their connection with large-scale atmospheric circulation patterns. Int J Climatol 36:4815–4830

Lee S, Min S (2018) Heat stress changes over East Asia under 1.5° and 2.0°C global warming targets. J Clim 31:2819–2831

Li X, Ren G, Wang S, You Q, Sun Y, Ma Y, Wang D, Zhang W (2021a) Change in the heatwave statistical characteristics over China during the climate warming slowdown. Atmos Res 247:105152

Li Y, Ding Y, Liu Y (2021b) Mechanisms for regional compound hot extremes in the mid-lower reaches of the Yangtze River. Int J Climatol 41:1292–1304

Liao W, Li D, Malyshev S, Shevliakova E, Zhang H, Liu X (2021) Amplified increases of compound hot extremes over urban land in China. Geophys Res Lett 48:e2020GL091252

Liu Q, Zhou T, Mao H, Fu C (2019) Decadal variations in the relationship between the Western Pacific Subtropical High and summer heat waves in East China. J Clim 32:1627–1640

Luca PD, Messori G, Faranda D, Ward PJ, Coumou D (2020a) Compound warm-dry and cold-wet events over the Mediterranean. Earth Syst Dyn Discuss 11:793–805

Luca PD, Messori G, Pons FM, Faranda D (2020b) Dynamical systems theory sheds new light on compound climate extremes in Europe and Eastern North America. Q J R Meteorol Soc 146:1636–1650

Lucarini V, Faranda D, Wouters J (2012) Universal behaviour of extreme value statistics for selected observables of dynamical systems. J Stat Phys 147:63–73

Luo M, Lau N (2017) Heat waves in southern China: synoptic behavior, long-term change, and urbanization effects. J Clim 30:703–720

Luo M, Lau N (2018) Increasing heat stress in urban areas of Eastern China: acceleration by urbanization. Geophys Res Lett 45:13060–13069

Matthews T, Wilby RL, Murphy C (2017) Communicating the deadly consequences of global warming for human heat stress. Proc Natl Acad Sci 114:3861–3866

Messori G, Faranda D (2020) Technical note: characterizing and comparing different palaeoclimates with dynamical systems theory. Clim past 17:545–563

Peng JB (2014) An investigation of the formation of the heat wave in Southern China in summer 2013 and the relevant abnormal Subtropical High activities. Atmos Ocean Sci Lett 7:286–290

Perkins SE (2015) A review on the scientific understanding of heatwaves: their measurement, driving mechanisms, and changes at the global scale. Atmos Res 164:242–267

Perkins SE, Alexander LV (2013) On the measurement of heat waves. J Clim 26:4500–4517

Perkins SE, Alexander LV, Nairn J (2012) Increasing frequency, intensity and duration of observed global heatwaves and warm spells. Geophys Res Lett 39:L20714

Qiao S, Chen D, Wang B, Cheung HN, Liu F, Cheng J, Tang S, Zhang Z, Feng G, Dong W (2021) The longest 2020 Meiyu season over the past 60 years: subseasonal perspective and its predictions. Geophys Res Lett 48:e2021GL093596

Ren X, Yang D, Yang X (2015) Characteristics and mechanisms of the subseasonal eastward extension of the South Asian High. J Clim 28:6799–6822

Reynolds RW, Rayner NA, Smith TM, Stokes DC, Wang W (2002) An improved in situ and satellite SST analysis for climate. J Clim 15:1609–1625

Robine J, Cheung SL, Le Roy S, Van Oyen H, Griffiths CE, Michel J, Herrmann FR (2008) Death toll exceeded 70,000 in Europe during the summer of 2003. CR Biol 331(2):171–178

Rousi E, Kornhuber K, Beobide-Arsuaga G, Luo F, Coumou D (2022) Accelerated western European heatwave trends linked to more-persistent double jets over Eurasia. Nat Commun 13:3851

Shang W, Ren X, Duan K, Zhao C (2019) Influence of the South Asian high-intensity variability on the persistent heavy rainfall and heat waves in Asian monsoon regions. Int J Climatol 40:2153–2172

Stéfanon M, D'Andrea F, Drobinski P (2012) Heatwave classification over Europe and the Mediterranean region. Environ Res Lett 7:014023

Takaya K, Nakamura H (1997) A formulation of a wave-activity flux for stationary Rossby waves on a zonally varying basic flow. Geophys Res Lett 24:2985–2988

Tang S, Qiao S, Wang B, Liu F, Feng T, Yang J, He M, Chen D, Cheng J, Feng G, Dong W (2023) Linkages of unprecedented 2022 Yangtze River Valley heatwaves to Pakistan flood and triple-dip La Niña. Npj Clim Atmos Sci 6:44

Tao SY, Zhu RK (1964) The 100-mb flow patterns in southern Asia in summer and its relation to the advance and retreat of the West Pacific subtropical anticyclone over the Far East. Acta Meteorol Sin 34:387–396

Wang W, Zhou W, Li X, Wang X, Wang D (2016) Synoptic-scale characteristics and atmospheric controls of summer heat waves in China. Clim Dyn 46:2923–2941

Wang B, Li J, He Q (2017) Variable and robust East Asian monsoon rainfall response to El Niño over the past 60 years (1957–2016). Adv Atmos Sci 34:1235–1248

Wang J, Feng J, Yan Z, Chen Y (2020) Future risks of unprecedented compound heat waves over three vast urban agglomerations in China. Earth's Future 8:e2020EF001716

Wei W, Zhang R, Wen M, Rong X, Li T (2014) Impact of Indian summer monsoon on the South Asian High and its influence on summer rainfall over China. Clim Dyn 43:1257–1269

Wei W, Zhang R, Wen M, Kim B, Nam J (2015) Interannual variation of the South Asian High and its relation with Indian and East Asian summer monsoon rainfall. J Clim 28:2623–2634

Xie S, Hu K, Hafner J, Tokinaga H, Du Y, Huang G, Sampe T (2009) Indian ocean capacitor effect on Indo-Western Pacific climate during the summer following El Niño. J Clim 22:730–747

Xie S, Du Y, Huang G, Zheng X, Tokinaga H, Hu K, Liu Q (2010) Decadal shift in El Niño influences on Indo-Western Pacific and East Asian climate in the 1970s. J Clim 23:3352–3368

Xie W, Zhou B, Han Z, Xu Y (2022) Substantial increase in daytime-nighttime compound heat waves and associated population exposure in China projected by the CMIP6 multi-model ensemble. Environ Res Lett 17:045007

Yang J, Liu Q, Xie S, Liu Z, Wu L (2006) Impact of the Indian ocean SST basin mode on the Asian summer monsoon. Geophys Res Lett 34:L02708

Yang K, Cai W, Huang G, Hu K, Ng B, Wang G (2022) Increased variability of the western Pacific subtropical high under greenhouse warming. Proc Natl Acad Sci USA 119(23):e2120335119

Zhang P, Liu Y, He B (2016) Impact of East Asian summer monsoon heating on the interannual variation of the South Asian High. J Clim 29:159–173

Zhang Q, Zheng Y, Singh V, Luo M, Xie Z (2017) Summer extreme precipitation in eastern China: mechanisms and impacts. J Geophys Res Atmos 122:2766–2778

Zhu Y, Wang H, Zhou W, Ma J (2011) Recent changes in the summer precipitation pattern in East China and the background circulation. Clim Dyn 36:1463–1473

Zi Y, Xiao Z, Yan H, Xu J (2021) Sub-seasonal east-west oscillation of the western pacific subtropical high in summer and its air-sea coupling process. Clim Dyn 58:115–135